Barkhausen noise: Elementary signals, power laws, and scaling relations

Djordje Spasojević,[1] Srdjan Bukvić,[1] Sava Milošević,[1,2] and H. Eugene Stanley[2]
[1]*Faculty of Physics, University of Belgrade, P.O. Box 368, 11001 Belgrade, Serbia*
[2]*Center for Polymer Studies and Department of Physics, Boston University, Boston, Massachusetts 02215*
(Received 29 January 1996; revised manuscript received 7 June 1996)

We report extensive measurements, with sufficiently large statistics, of the Barkhausen noise (BN) in the case of the commercial VITROVAC 6025 X metal glass sample. Applying a very scrutinized numerical procedure, we have extracted over one million of the BN elementary signals from the raw experimental data, whereby we made a rather precise estimation of the relevant power law exponents. In conjunction with the experimental part of the work, we have recognized a generic shape of a single BN elementary signal (BNES), and we have put forward, without invoking any existing model of BN, a simple mathematical expression for BNES. Using the proposed expression for BNES in a statistical analysis, we have been able to predict scaling relations and an elaborate formula for the power spectrum. We have also obtained these predictions within the generalized homogeneous function approach to the BNES's probability distribution function, which we have substantiated by the corresponding data collapsing analysis. Finally, we compare all our findings with results obtained within the current experimental and theoretical research of BN. [S1063-651X(96)13409-7]

PACS number(s): 05.40.+j, 75.60.Ej, 05.90.+m, 02.50.Wp

I. INTRODUCTION

The Barkhausen noise (BN) is a classical physical phenomenon which is manifested as a series of jumps in magnetization of a ferromagnetic sample when it is exposed to a varying external magnetic field. These changes induce voltage changes in a surrounding coil, and consequently they can be transformed into acoustic noise. Since its discovery [1], BN has been incessantly investigated (see, for instance, the reviews [2–4]) because of its vast practical importance (such as for various types of magnetic recordings [5] and for noninvasive material characterization techniques [6]) and because of its major conceptual importance for understanding dynamics of ferromagnets on the magnetic domain scale. These investigations have shown that BN is a very complex physical phenomenon with many different appearances which depend on kind of ferromagnetic specimen under study, character of quenched in defects, external field driving rate, thermal effects, strength of the demagnetization fields, and other experimental details.

At present there are several conceptually different (and to a certain extent incoherent) theoretical approaches to the explanation of BN. The first of the current theoretical approaches we would like to bring forward here is that one which analyzes BN as a consequence of the domain-wall (DW) motion. Accordingly, BN has been investigated via a single-degree-of-freedom model [7] in which individual DW is moving (in a random walk manner) through a spatially random coercive field. The Langevin equation approach [7] has been developed further in a number of papers [8–10] and thoroughly reviewed by Bertotti [11,12]. In a different approach, the DW motion and domain nucleation have been experimentally and theoretically investigated in relation to BN in ultrathin ferromagnetic films [13].

Recently, the concept of the self-organized criticality (SOC) [14,15] has acquired a distinguished role in the contemporary BN investigations. Since the appearance of the SOC concept, many questions related to its application to BN has been raised which initiated many different studies and even antagonistic interpretations. The applicability of the SOC concept to BN was investigated by Meisel and Cote [16,17] who offered qualitative arguments and specific measurements (in various materials, starting with a metal glass sample) in support to the relevance of the SOC concept for the explanation of BN. They augmented their arguments by performing the Jensen, Christensen, and Fogedby (JCF) type of analysis [18] of statistical characterization of the observed BN. Besides, the avalanchelike topological rearrangements of cellular domain patterns in magnetic garnet films were investigated by Babcock and Westervelt [19], who interpreted the obtained findings in the framework of the SOC concept. Finally, BN has been investigated as a fractal time signal [20] and subsequently simulated via a SOC model [21] by Geoffroy and Porteseil.

Concurrently, there are approaches that put under doubt the relevance of the SOC concept to BN. Thus, O'Brien and Weissman [22] have pointed out that the $1/f$ noise and power-law distributions are not necessarily evidences of SOC, but rather the consequences of scaling properties of quenched disorder in material. In this spirit, they have performed experimental and computational analyses of the fourth-order signal correlations (dubbed the second spectra), which was expected to reveal violations of the detailed balance in self-organization caused by an external driving. The main conclusion of these analyses is that the most statistical characterization of BN is consistent with the single-degree-of-freedom models of Allesandro *et al.* [7]. On the other hand, within a many-degree-of-freedom model approach [23–25], it has been recently argued that features of BN can be adequately described by the zero-temperature random-field Ising (RFI) model, and that the observed scaling in BN should be a consequence of the vague proximity to a plain old critical point (which in the model studied is determined by a critical value of the width of the random-field distribution [24]). The role of material defects for the explanation of BN has been also emphasized in the approach of Urbach

et al. [26], who exploited concept of rough-surfaces growth to describe the DW motion, with the conclusion that long-range demagnetization fields strongly affect the character of BN.

Despite the vast list of the BN facets that have been investigated, so far the question whether the BNES's probability function is a generalized homogeneous function (GHF) has not been widely attacked and analyzed. Similarly, there has been a little attention payed to the form of individual BN signals and consequences which their form might have to the global BN. In this paper, we report on extensive measurements (with sufficiently large statistics) of BN in the case of a commercial VITROVAC 6025-X metal glass sample. In the course of these measurements, we have introduced many experimental precautions and scrutinized numerical methods in order to eliminate effects of the extrinsic noise. In this way, we have been able to extract a proper average form of the individual BN signals from the experimental data and, what is more important, to provide evidences that the BNES's probability distribution is a GHF. Our theoretical treatment of the problem has been first focused on investigation of power-law behaviors of BN and their relations with an analytical expression which describes the obtained average shape of BNES's. After providing qualitative theoretical arguments which support the accepted signal form, we have carried out an analysis of the JCF [18] type (which does not take into account any specific origin of the noise signal), and we have obtained various scaling relations (satisfied upon inserting the experimental values of scaling exponents), as well as an expression for the power spectrum whose numerical presentation is in agreement with our experimental results. Then, we have analyzed the hypothesis that the BNES's probability distribution function is a GHF and we have expounded on consequences which such an assumption implies. Thus, it appears that power-law behaviors of BN, and, in particular, all scaling relations can be obtained as consequences of the GHF property of the BNES's probability distribution function and that other consequences, such as the data collapsing of numbers of events, can serve as adequate experimental confirmations of the GHF hypothesis.

This paper is organized as follows. In Sec. II we first describe our experimental setup. Then we elaborate on the numerical procedure utilized for analysis of the recorded data, and present our experimental results. In Sec. III we develop our inductive theoretical approach to BN and present a detailed comparison of the theoretically and experimentally obtained results. In Sec. IV, we provide evidences that the BNES's probability distribution function is a generalized homogeneous function which enable us to rederive all scaling relations (obtained in Sec. III) in the spirit of the standard critical phenomena. Finally, we give an overall discussion of the utilized experimental method and the unfolded theory within the present knowledge about the Barkhausen noise.

II. EXPERIMENTAL ANALYSIS

A. Experimental setup

We have used the experimental setup which is schematically depicted in Fig. 1, and here we give a brief description of the parts of the setup. A signal generator (Krohn-hite 5400

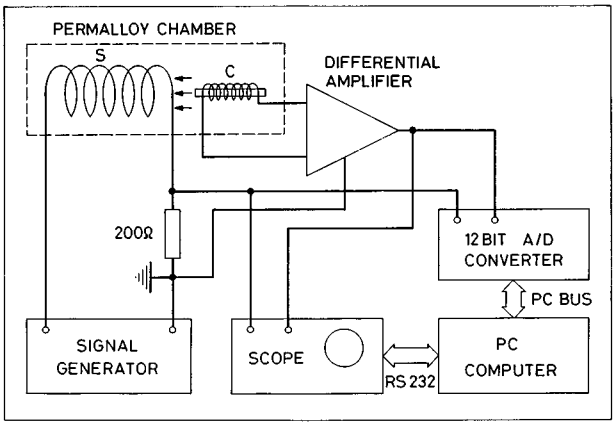

FIG. 1. A schematic depiction of the setup used in the experimental course of this work. The ballast resistor of 200 Ω has been used to reduce the influence of Barkhausen noise on the current which flows through the driving solenoid S.

B) provided sinusoidal current for the driving solenoid S which produced a magnetic field, $H=H_0\sin(2\pi f_0 t)$, that continuously drew a specimen (located within the pickup coil C) through a B-H loop. A small driving frequency $f_0=0.03$ Hz has been used to prevent (or, more precisely, to reduce significantly) overlapping of the Barkhausen pulses. The length of the solenoid S was 20 cm, while its inner diameter was 5 cm, and it consisted of 675 turns of a copper wire (0.5 mm in diameter). The maximal strength of the magnetic field H_0, produced by S, was about 160 A m^{-1} (which is approximately four times larger than the mean Earth magnetic field), and this small field was oriented orthogonally to the local Earth magnetic field.

We have performed our measurements on a quasi-two-dimensional as-cast metal glass sample (a commercial VITROVAC 6025 X produced by Vacuum Schmeltz), with linear dimensions 4 cm × 1 cm × 0.003 cm. The Barkhausen pulses [see Fig. 2(a)], which correspond to the jumps in magnetization of the specimen, were collected as induced voltage pulses via the pickup coil C (of length 5.5 cm, with rectangular cross section 12 mm× 2 mm). The specimen was placed inside the coil in such a way that there was no mechanical tension. The pickup coil C, with the resistance $R=30$ Ω, comprised of 300 turns of copper wire and its magnetic coupling with S was weak. The pickup coil C, as well as the inserted specimen, were placed in the middle of the solenoid S.

Electric signal from the pickup coil C has been amplified (with a gain of 2000) through a low-noise differential amplifier. Trains of the Barkhausen pulses were monitored, together with the driving current, on a HAMEG 205-3 digital storage scope. In order to improve quality and the duration of the recorded signal, an analog-to-digital (A/D) converter (made by Electronic Design, model ED 2000 with high-speed module ED 2019, compatible with the Burr-Brown card, model PCI-20023M-1), with the 12-bit resolution, has been used for the data collection. The A/D converter had the input range −5 V to +5 V, with the maximal rate of 300 000 samples per second, permitting, in a single run, collection of as many samples as the computer memory could accept. We have found that the sampling rate of 200 000 samples per

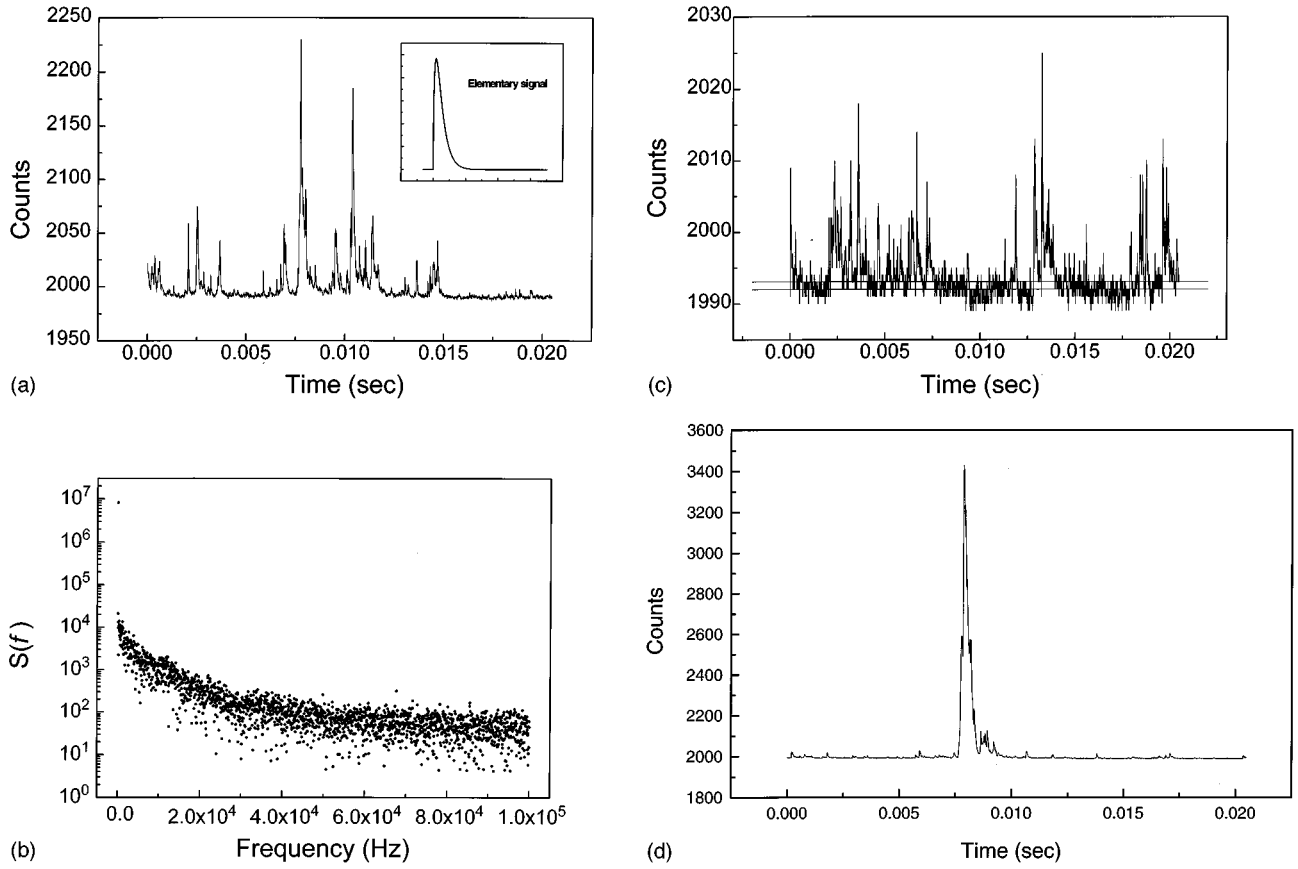

FIG. 2. (a) A typical train of Barkhausen pulses observed in an as-cast commercial VITROVAC 6025 X metallic glass ribbon (with linear dimensions 4 cm×1 cm×0.003 cm). The train is presented by the line drawn through 4096 points (of digitized voltage, recorded at the sampling rate of 200 000 samples per second). The unit on the ordinate axis is 1 count of the A/D converter, which is equivalent to the voltage of 5/2048 V. The huge offset, of about 2000 counts, appears as a consequence of the fact that the voltage of 0 V corresponds to the 2048th count of the A/D converter. For the sake of comparison, an elementary signal of the form (8) is presented in the inset (where the time and voltage units are arbitrary). (b) Power spectrum (in arbitrary units) of the train of Barkhausen pulses shown in the preceding graph. The high value (close to 10^7) of the $f=0$ harmonic is a consequence of the huge offset of the recorded train of pulses. (c) The positions of baseline (the lower horizontal line parallel to the time axis) and the discrimination level (the upper horizontal line) for a nontypical train of Barkhausen pulses. The nontypical train of small Barkhausen pulses has been chosen here intentionally since the two lines (the baseline and the discrimination level) would be otherwise indistinguishable in a figure that would present a typical train of Barkhausen pulses. (d) A huge single Barkhausen signal which lasted 0.002 sec (located, approximately, between 0.0075 sec and 0.0095 sec).

second provided a good balance between resolution of peaks and the number of peaks recorded during a single run. With respect to this problem, we would like to emphasize that the amplifier cutoff frequency (100 kHz) has been chosen to prevent aliasing effect in the power spectrum [27].

The achieved quality of the Barkhausen noise measurement, obtained in the way described above, was accompanied by undesirable sensitivity to the low-level electric and magnetic extrinsic noise. To minimize this concomitant noise, the driving solenoid S, the pickup coil C, and the amplifier, were enclosed in a double-wall Permalloy Chamber (made by Vacuum Schmeltz), which reduced the external magnetic fields (including the Earth's magnetic field), at least by a factor of 10 000. Finally, a copper chamber (which is not shown in Fig. 1) has been used as an additional Faraday cage to minimize external electric fields. As a result, amplitude of the overall extrinsic noise was not larger than 4 counts of the A/D converter, that is, signal-to-noise ratio was about 500. Finally, the care was taken so as to record the entire set of data at the constant temperature equal to 20 °C.

B. Numerical processing of recorded data

We drove the sample studied through B-H loop for 10 h before any recording was done, in order to achieve the stationary regime of the hysteresis loop cycling. Then, we have collected our experimental data in a small interval of H (centered at the value $H=0$), which encloses the corresponding coercive field H_c owing to the fact that our specimen is a soft magnet. During a single recording, which lasted about 0.6 sec, we got 128 kB of data (131 072 points of the digitized voltage), and we present here results of statistical averaging over 200 successive single recordings obtained (within 2 h of measurement) under identical experimental conditions. In Fig. 2(a) we present a typical train of Barkhausen pulses by the line drawn through a set of 4096 successively recorded points. The presented set belongs to one of the 200 single

recordings, while the time counting has been shifted, for the sake of convenience, to the beginning of the train of pulses. One can notice that in the recorded train there are several clusters of big pulses and a multitude of small pulses hardly distinguishable from the concomitant extrinsic noise.

After the data collection, we have performed numerical processing of the raw recorded data. There are several reasons for this processing. First, the data collected by the pickup coil were of millivolts in magnitude, and they had to be amplified in order to be adjusted to the input range of the analog-to-digital converter. The applied signal amplification inevitably introduces various types of distortions since the amplified signal is the convolution of the amplifier characteristic and of the input signal power spectrum. These distortions are potentially of the greatest influence on the most frequent short-lasting, and small (in magnitude), signals. To eliminate these distortions, we have performed a deconvolution procedure, using the fast Fourier transform (FFT) method, based on known characteristic of the amplifier used. Within this procedure, it was possible to introduce cutoff at any desired frequency (below the imposed hardware frequency cutoff), and we have investigated the influence of the frequency cutoff choice. Thus, we have found that the data, important for the further analysis, remain stable under variation of the frequency cutoff, and, for this reason, in what follows we present our results obtained for the deconvolved data with the cutoff frequency set at the hardware value 100 kHz.

The necessity for the numerical processing of the original data stems also from the inevitable presence of undesirable extrinsic noise. There are many kinds of extrinsic noise, such as the exterior fields, the thermal noise, the electric network noise, and the noise that originates from the computer components. The presence of the undesirable noise can be noticed in the power spectrum of the typical unprocessed signal, which appears as the white noise at frequencies higher than 50 kHz [see Fig. 2(b)]. In order to reduce the effect of the extrinsic noise, we have applied the Wiener filtering method [27], but it turned out to be an excessive step, that is, it did not change final results, which can be explained by the relatively high signal-to-noise ratio. One can also see in Fig. 2(b) that there is no so-called aliasing effect (which was eliminated by the suitable choice of the amplifier cutoff frequency).

In the concluding part of this subsection, we shall provide a usable definition of a single BN signal within the recorded trains of pulses. To this end, we first have to define baseline of a train of pulses. It appears to be most appropriate to choose for a baseline the horizontal line, in the counts (of voltage) vs time plane, which has maximum number of intersects with the train line. In other words, the baseline corresponds to the count b_l of the A/D converter that most frequently occurs in a given train of pulses (this definition is correct only in a case of a slowly varying external field). Having defined the baseline, we point out that above this line there are both the BN pulses and the extrinsic noise pulses, whereas below the baseline one can find only pulses of the extrinsic noise (if we neglect the inverse BN pulses, which appear to be almost improbable events under the described experimental conditions). Hence, we can numerically analyze the extrinsic noise pulses which appear below the baseline, and, in particular, we can thereby estimate the corresponding extrinsic noise standard deviation σ (supposing that the noise is symmetrical in respect with the baseline). To discriminate the BN pulses from the extrinsic noise, we establish a discrimination level at the value $b_d = b_l + \delta_d$, where δ_d is a quantity that is proportional to σ [see Fig. 2(c)]. In what follows, we present all our results for $\delta_d/\sigma = 1$ (with a comment that our analysis for the power law exponents has shown that they are not sensitive to particular values of the ratio δ_d/σ). Finally, we define as a single BN signal each part of the recorded line of pulses above the discrimination level that ranges between its two consecutive intersections with the discrimination level [see, for instance, a huge BN signal presented in Fig. 2(d)]. Applying the foregoing procedure, we have extracted 1 078 796 elementary signals from the experimental data, which has rendered the basis for our statistical analysis.

C. Experimental results

Three basic physical quantities that describe a single BN signal are signal duration, area of the signal, and energy released during the signal occurrence. To define these quantities, we denote BN by $F(t)$ as a function of time t. The signal duration T is the time interval, between the first t_f and the last moment t_l, in which the signal is above the discrimination level. The area of a signal A is the area between signal and the baseline b_l, which can be written in the form $A = \int_{t_f}^{t_l} [F(t) - b_l] dt$, and which is proportional to the sum of the ordinates of the discrete form of the function $F(t) - b_l$. Physically, the area of a signal is proportional to the change in the specimen magnetization occurring during the signal duration. Finally, the signal energy E is proportional to the integrated squared signal, that is, $E \propto \int_{t_f}^{t_l} [F(t) - b_l]^2 dt$.

The self-similar appearance of the experimental results for BN [Fig. 2(a)] implies that there should exist various scaling laws, and in this spirit one can expect that the probability distributions $P(T)$, $P(A)$, and $P(E)$, of the three quantities defined in the preceding paragraph, should be of the power-law type

$$P(T) \sim T^{-\alpha}, \quad P(A) \sim A^{-\tau}, \quad P(E) \sim E^{-\epsilon}, \tag{1}$$

where α, τ, and ϵ are the corresponding critical exponents. Our experimental results related to these distributions are presented in Figs. 3–5, respectively, from which we obtain the following values for the critical exponents

$$\alpha = 2.22 \pm 0.08, \quad \tau = 1.77 \pm 0.09, \quad \epsilon = 1.56 \pm 0.05. \tag{2}$$

Besides the distributions (1), within a complete analysis, it is important to establish the joint distributions, which in practice means to find joint histograms. Thus, in Fig. 6 we present a log-log plot of our experimental results in the form: signal area vs signal duration, which means that every point in the figure represents a single BN signal. Similarly, in Fig. 7 and Fig. 8 we present joint histograms for energy-duration and energy-area distributions, respectively. From these three figures, one may gain insight into the joint probabilities $P(A,T)$, $P(E,T)$, and $P(E,A)$, as they are approximately proportional to the number of points per unit area in the

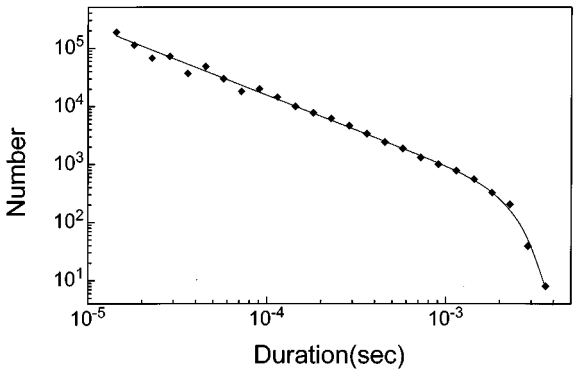

FIG. 3. Experimental data for the distribution of signal durations (diamonds) and the pertinent best fit of the form (15)–(16) (solid line). The scaling region, almost two decades long, can be recognized, and can be described by the critical exponent $\alpha=2.22$. To obtain this distribution of signal durations, the original data were first grouped into logarithmically spaced bins, and one can notice that, despite the huge number of collected data, there appears an unavoidable scattering of the points in the region of signals having short durations. This fact is a consequence of the incompatible discreteness of the two quantities — the originally measured signal duration and the magnitude of bins.

respective planes. In addition, from the same figures, one can see that the corresponding pairs of quantities are not related by single functions [for instance, in the simple form $A=f(T)$], although, on the other hand, one may see that each pair displays a significant linear correlation in the log-log plot. Therefore, it is appropriate to assume validity of the following power laws:

$$A\sim T^{\gamma_1}, \quad E\sim T^{\gamma_2}, \quad E\sim A^{\gamma_3}. \tag{3}$$

The least-square fit of our data gives the following values for the critical exponents:

$$\gamma_1=1.51\pm0.01, \quad \gamma_2=2.03\pm0.02, \quad \gamma_3=1.36\pm0.01. \tag{4}$$

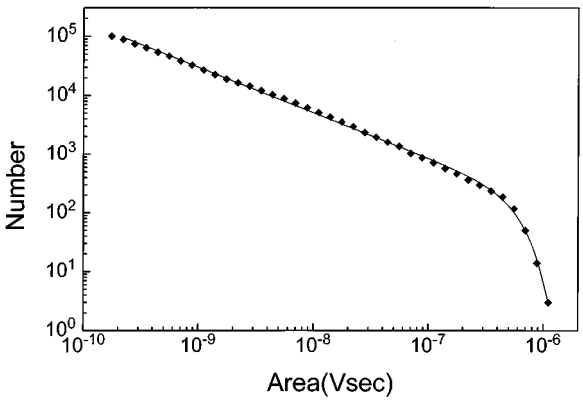

FIG. 4. Experimental data for the distribution of signal areas (diamonds) and the best fit curve [of the power-law type, with the correction factor of the form (22)]. The critical exponent $\tau=1.77$ describes the scaling region.

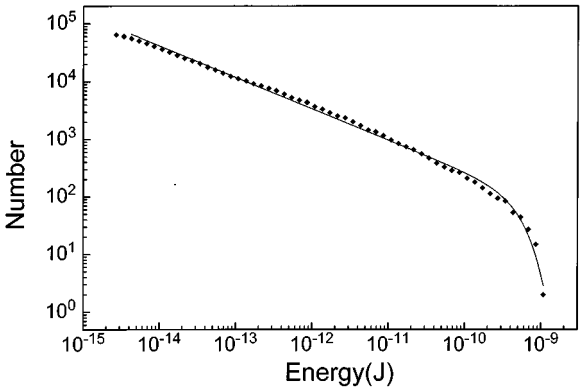

FIG. 5. Experimental data for the distribution of signal energies (diamonds) and the best fit curve [of the power-law type, with the correction factor of the form (27)]. The critical exponent $\epsilon=1.56$ describes the scaling region.

We have tested the validity of assumption (3), that is, of the corresponding linearity in the log-log plots, by evaluating the pertinent linear correlation Pearson's coefficients

$$r(A,T)=0.946, \quad r(E,T)=0.871, \quad r(E,A)=0.988, \tag{5}$$

which appears to be satisfactorily high since in the ideal case these coefficients should be equal to one [27]. Furthermore, we have calculated the more informative Spearman rank-order correlation coefficients

$$r_s(A,T)=0.886, \quad r_s(E,T)=0.783, \quad r_s(E,A)=0.985, \tag{6}$$

which again turns out to be satisfactorily high, as it is known that in an ideal case these coefficients should be equal to one

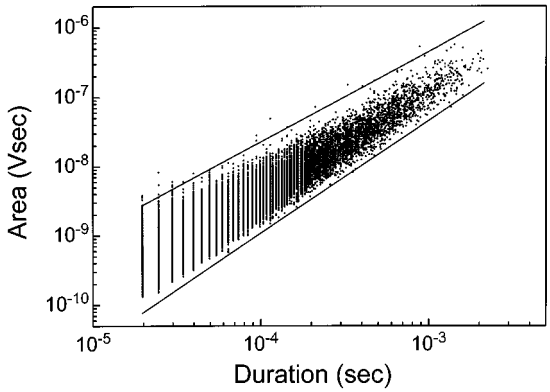

FIG. 6. Area vs duration data of the BN signals (or the so-called joint area-duration distribution). Almost all experimentally obtained points (dots) lie within the domain bounded by the two solid lines, which correspond to the estimates $\gamma_{min}=1.3$ and $\gamma_{max}=1.63$ that were achieved using these data and the theoretical prediction (9). We point out here that the presented data are taken from the first 50 single recordings (of the total number of 200 single recordings) because a presentation of all available data would give a completely black central region.

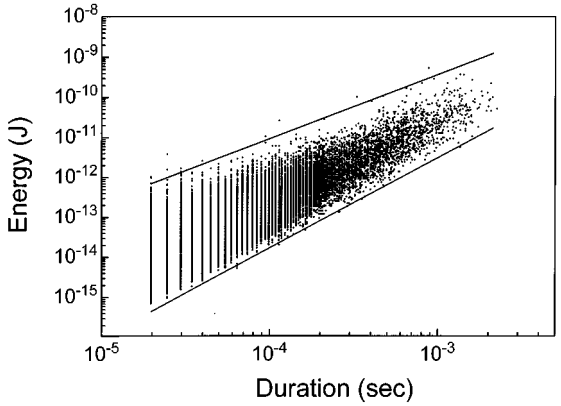

FIG. 7. Energy vs duration data of the BN signals (or the so-called joint energy-duration distribution). Almost all experimentally obtained points (dots) lie within the domain bounded by the two solid lines obtained through (10) and the estimates γ_{min} and γ_{max} quoted in the caption of Fig. 6. The comment made at the end of the Fig. 6 caption applies here as well.

[27]. Thus, we may conclude that results (5) and (6) of both tests confirm that our experimental data do satisfy the power laws (3).

Finally, one of the main characteristics of BN is a power-law spectrum of the type $S(f)\sim 1/f^{\beta}$. In Fig. 9 we present the power spectrum of the observed BN (deconvolved from the amplifier characteristic), which has been obtained by applying the FFT method. More specifically, we have applied the numerical procedure described in the book [27] under the name SPCTRM (using the option that assumes signal overlapping and the Parzen window). Within this procedure we have worked on the 4096-point segments, obtaining thereby 2048 harmonics in the power spectrum. Our final results display linearity, over almost two decades in the log-log plot (see Fig. 9), with a slight curvature at the beginning (in the low-frequency region). We have estimated that the exponent β, which should describe the linearity region, lies between 1.6 and 1.7. This shows that BN is neither the pink type

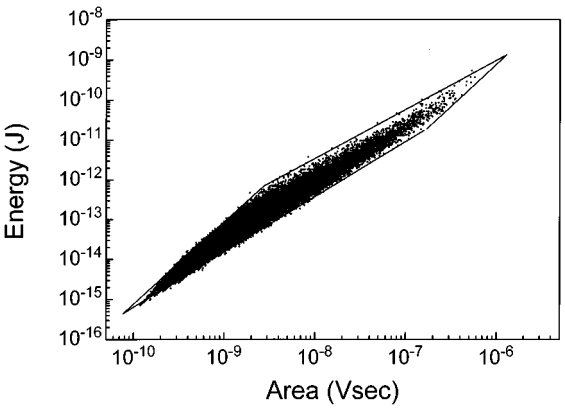

FIG. 8. Energy vs area data of the BN signals (or the so-called joint energy-area distribution). In this case, one can also notice that almost all experimentally obtained points (dots) lie within the domain bounded by the four solid lines, which were obtained using relation (12) and the estimates γ_{min} and γ_{max} quoted in the caption of Fig. 6.

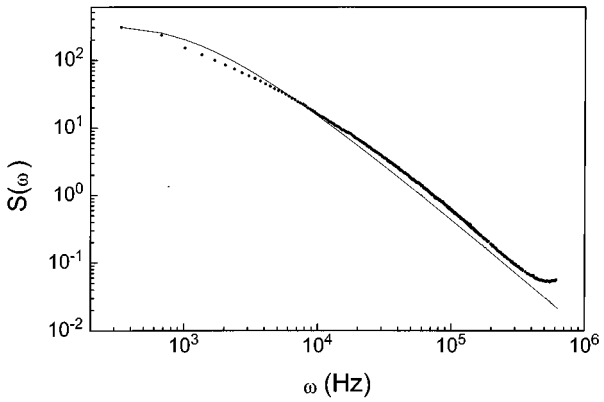

FIG. 9. Power spectrum $S(\omega)$ (in arbitrary units) of the observed BN signals. The set of points (dots) is calculated via the FFT method and represent experimental findings, whereas the solid curve represents numerical evaluation of (38).

noise ($\beta=1$) nor the Brownian type noise ($\beta=2$). A comparison of this result with results found by other authors will be given in Sec. IV.

III. THEORETICAL ANALYSIS

In this section, we propose a theoretical approach performed along the lines of the approach developed by Jensen, Christensen, and Fogedby [18], which has been widely used in previous analyses of experimental results in the case of systems that exhibit SOC-like behavior. This is an inductive approach whose virtues will be discussed in the next section, simultaneously with expounding a phenomenological scaling approach. Accordingly, let us consider the family $\mathcal{B}$ of the pertinent uncorrelated (elementary) time signals each labeled by index i, with time profile $f_i(t')$ (where t' is supposed to be measured from the moment of beginning of the elementary signal), and the (total) recorded time signal $F(t)$ (which is a stochastic sum of the elementary signals that start at random times with overall rate ν). Then, if $p_i(n\delta)$ is the indicator function (which is equal to one if an elementary signal of the type i has started at the instant of time $n\delta$, and otherwise it is equal to zero), $F(t)$ can be expressed in the form

$$F(t)=\sum_i \sum_{n=-\infty}^{+\infty} f_i(t-n\delta)p_i(n\delta), \tag{7}$$

which shows that $F(t)$ is a stochastically stationary time signal. In our study, we accept that BN is a time signal of type (7), assuming that BN is observed in a time interval which is, on the one hand, practically infinite (compared to average duration of BN elementary signals), and, on the other hand, short enough (compared to the period of the driving magnetic field) that one can consider the observational conditions uniform and elementary signals uncorrelated. Furthermore, we assume that the experimentally recorded single BN signals are effectively elementary BN signals, which should be correct if the number of those single signals that are comprised of several elementary signals glued together is statistically irrelevant.

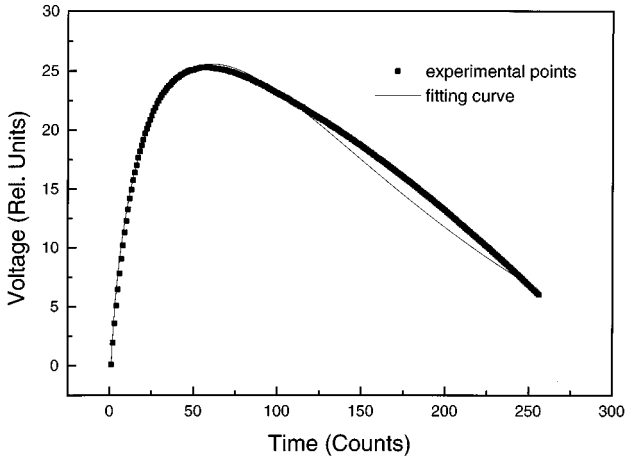

FIG. 10. The average form of BNES's (solid squares) obtained through an analysis of the experimental data, whose main step consisted in rescaling of the BNES's shapes to the same (constant) duration and the same (constant) area. The continuous line represents the accepted analytical form (8), with $\gamma=1.51$, and $T=119$ time counts in $g(t'/T)=\exp(-t'/T)$.

Power-law behavior related to the time signal $F(t)$ of the type (7) depends on the characteristics of the distribution of elementary signals. It may happen that there exists some prominent subfamily of elementary signals (having specific shape) such that it has a dominant statistical weight in the distribution of elementary signals. In such a case, performing statistical analysis, one can neglect the presence of elementary signals which do not belong to the subfamily and try to relate the properties of the time signal $F(t)$ to the specific shape of the subfamily elementary signals. A visual inspection of the typical train of elementary signals [see Fig. 2(a)] can hardly detect existence of a subfamily of specific signals. However, a more elaborate numerical investigation of the available experimental data can demonstrate that a subfamily in fact exists. To this end, one should first rescale each BNES $f_i(t')$ (by appropriate dilation, or contraction, of its duration time and voltage amplitude) so that the rescaled signal $f_i'(t')$ acquires unit duration and area, which eventually makes signals' shapes suitable for mutual comparison. Then, one should perform a straightforward averaging of the rescaled signals within its own set, so that the value $f_a(t')$ of the function obtained in this way, at the moment t', is the average of $f_i'(t')$.

In practice, we have analyzed all BNES's which belong to the scaling region (see Fig. 3), that is, which have durations between 16 and 256 time counts of the used A/D converter. Then, we have rescaled all BNES's to the duration of 256 time counts, by linear interpolation, and we have dilated (contracted) them along the voltage axis, in such a way that the maximal height of the rescaled BNES's must not exceed 256 voltage counts, and, furthermore, so that the all rescaled BNES's acquire a same area. Finally, we have performed the averaging of the rescaled BNES's and the resulting shape [function $f_a(t')$] we present in Fig. 10 as a set of 256 discrete points.

The conclusion of the described analysis emerges as the statement — although the shapes of BNES's appear irregular, there exists a generic smooth signal form such that BNES's are on average of the same type (see Fig. 10). For the corresponding analytical form we propose

$$f(t')=\begin{cases} Ct'^{\gamma-1}g(t'/T), & t'>0 \\ 0, & t'\leqslant 0\,, \end{cases} \tag{8}$$

where C is a proportionality constant, γ is the corresponding signal exponent, and $g(t'/T)$ is some function which is close to one for small values of the argument and falls rapidly to zero for large values of t'/T. Here, t' is the time measured from the moment of the beginning of the elementary signal, and T is a characteristic time that can be thought of as the duration of the elementary signal. Here we would like to point out that our analysis will show that the final results are most sensitive to the raising part of the signal, that is, to the factor $t'^{\gamma-1}$. In other words, it will turn out that a specific form of $g(t'/T)$ does not have an essential role, and, for the sake of completeness, in the later numerical investigations we shall use the exponential decay form $g(x)=\exp(-x)$. The accepted kind of elementary signal is depicted in the inset of the Fig. 2(a), where it can be compared with the recorded signals (this type of the signal is also in accordance with forms experimentally observed by other authors; see, for instance, Fig. 10 of the second paper of O'Brien and Weissman [22], and Fig. 1 presented by Urbach *et al.* [26]).

Physical reasons for choosing (8) for the average shape of BNES can be complemented by the following qualitative arguments. In the study of BN we follow changes in the domain structure caused by changes in external magnetic field. First, we observe that the domain structure of a magnetic specimen is stochastically organized due to the complex interplay of local fields, internal stresses, and bulk and surface defects. For a given field the structure is stationary, whereas small changes of the field are prone to trigger avalanchelike rearrangements of clusters of domains, which is usually initiated at a single domain. There are experimental evidences (see, for instance, Refs. [13] and [19]) that lead us to assume that the clusters which take part in an avalanchelike process comprise a fractal pattern, whose fractal dimension we identify with the signal exponent γ. Furthermore, we accept that an avalanchelike process is recorded as a single BN signal, and that the time evolution of the avalanche determines the shape of an elementary signal. The raising part of the signal is dominated by the advancement of the avalanche front (whose fractal dimension is equal to $\gamma-1$), and consequently there appears the factor $t'^{\gamma-1}$ in (8). Of course, after the rapid growth, the signal has eventually to die out, and the way it halts is described by the factor $g(t'/T)$. An exponential decay form for $g(t'/T)$ might be associated with the eddy-current damping, while the constant C can be thought of as a quantity proportional to the velocity of the advancement of the avalanche front.

The first three predictions that follow from the assumption (8) are the relations between duration, area, and energy, of an elementary signal:

$$A=CT^{\gamma}\Gamma(\gamma), \tag{9}$$

and

$$E = C^2 \left(\frac{T}{2}\right)^{2\gamma-1} \Gamma(2\gamma-1), \tag{10}$$

where

$$\Gamma(\gamma) = \int_0^\infty x^{\gamma-1} g(x)\, dx, \tag{11}$$

which, for the specific form $g(x) = \exp(-x)$ is in fact the standard gamma function. Then, eliminating duration T from (9) and (10), one obtains the relation

$$E = \frac{C^{1/\gamma}\Gamma(2\gamma-1)}{[2^\gamma \Gamma(\gamma)]^{2-1/\gamma}} A^{2-1/\gamma}, \tag{12}$$

between the energy and the area of an elementary signal. Once derived, the relation (9) may be considered as the defining relation the for signal exponent γ of BNES, providing that the constant C is known [see Eq. (13)]. Thus, the signal exponent γ can be conceived as a quantity which discriminates between the possible shapes of BNES's, and in what follows we accept such an attitude.

Analyzing our experimental findings, we came to the conclusion that the BN signal duration T and the signal exponent dimension γ should be considered as the two stochastic quantities, and we denote their joint distribution by $P(\gamma, T)$. By inspection of Figs. 6–8, one may also conclude that the distribution $P(\gamma) = \int P(\gamma, T)\, dT$ should be rather narrow, ranging between some lower limit γ_{min} and upper limit γ_{max}. Using the data for the joint distribution of the BN signal area A and duration T (see Fig. 6), we have estimated these two limits and the constant C of (8):

$$\gamma_{min} = 1.30 \pm 0.03, \quad \gamma_{max} = 1.63 \pm 0.03,$$

$$C = 0.004 \pm 0.001. \tag{13}$$

Thus, one may conclude that the BN signals should be distributed, with respect to their area and duration, between the two boundaries depicted in Fig. 6, which are obtained by substituting the values of C, γ_{min} (for upper border line) and γ_{max} (for lower border line) into (9). Furthermore, using (10), (12), and (13), we have obtained, in the same manner, the boundaries depicted in Fig. 7 and Fig. 8 for the energy-duration and energy-area joint distributions of the BN signals, respectively. The achieved rather precise prediction for boundaries of the energy-duration and energy-area distributions of BN signals (obtained through quantities estimated from the area-duration distribution) serves as a confirmation of validity of the assumed form (8) for an elementary signal.

The next question, which we are going to answer, is whether one may consider the two stochastic quantities γ and T as two independent stochastic quantities. With this aim in view, we have evaluated $P(\gamma|T)$, the conditional probabilities to observe an elementary signal with the signal exponent γ under condition that its duration is equal to T, from our experimental data and from the relation (9). The result of the corresponding evaluation, for six logarithmically spaced T bins [chosen within the scaling region of $P(T)$ distribution] is shown in Fig. 11. It should be observed that for all specific values of T, the conditional probabilities $P(\gamma|T)$

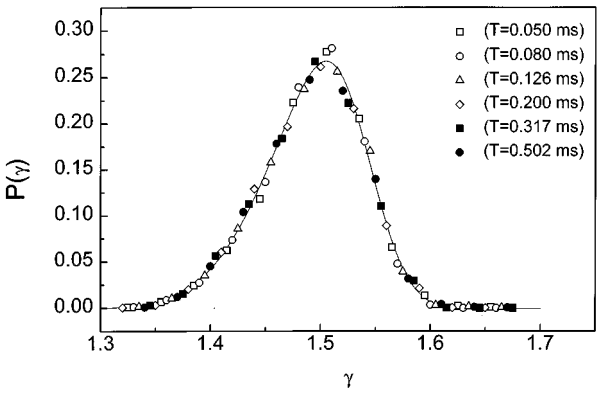

FIG. 11. Distribution of the signal exponent γ for six logarithmically spaced time bins which all belong to the scaling region of the BN signal duration distribution. One should observe that, for all specific values of T, the presented distributions collapse on a single curve, which has been fitted by the solid line (obtained through the Jandel Scientific Table Curve 2D program). The presented distribution may be rather well described as a Gaussian distribution with the mean and the halfwidth being equal to 1.4975 and 0.05, respectively.

collapse on the single curve. On these grounds, one can justifiably consider γ and T as the two independent stochastic quantities, which implies $P(\gamma|T) = P(\gamma)$ and $P(\gamma, T) = P(\gamma)P(T)$. As regards the distribution $P(\gamma)$, it can be described as a Gaussian (with the mean and the halfwidth σ_γ equal to 1.4975 and 0.05, respectively), although its identification with some of known distributions is of no major importance for our present analysis.

Our further analysis can be simplified by the fact that we can identify γ_1, given by (3) and (4), with the most probable value of the signal exponent associated with the distribution $P(\gamma)$. This identification can be justified by the high value of the relevant Pearson coefficient, given in (5), as well as by the fact that the peak of the distribution $P(\gamma)$ occurs at $\gamma = \gamma_1$ (see Fig. 11). Consequently, from (9), (10), and (12), follow the power laws of the type (3) and the scaling relations

$$\gamma_2 = 2\gamma_1 - 1, \quad \gamma_3 = 2 - \frac{1}{\gamma_1}. \tag{14}$$

Hence, we can see that the values 2.02 and 1.34, for γ_2 and γ_3, respectively, which follow from (14) and experimentally found value $\gamma_1 = 1.51$, are in a very good agreement with the values quoted in (4), which corroborates the scaling relations (14).

To complete the set of the expected scaling relations we find it appropriate to specify the first power law of (1) by introducing a correction factor

$$P(T) = B_t(T) T^{-\alpha}, \tag{15}$$

which is assumed to describe more accurately the signal distribution with respect to the signal duration T. Here, the introduced correction factor $B_t(T)$ should be constant in the scaling region, while for large T it should depend on T in such a way to describe the observed cutoff behavior (see Fig.

3). We are going to use the following phenomenological stretched-exponential form for the correction factor:

$$B_t(T)=B_{0t}\exp[-(T/T_c)^{1/\sigma_t}], \tag{16}$$

where B_{0t} is a constant, T_c is a characteristic cutoff time, and σ_t is the corresponding exponent. The stretched-exponential form (16) has been used in a similar content in the work [24], and its relevance to the phenomenon studied has been argued also by Alessandro *et al.* [7]. To assert values of the constants in (16), we have minimized χ^2 of our experimental data and the form (15) performing the Nelder-Mead downhill simplex method in multidimensions (see Ref. [27] and the program Amoeba given therein). Here we remind the reader that we have grouped our data into logarithmically spaced bins, so that the number $N(T_0)$ of single BN signals in a bin centered at T_0 is given by

$$N(T_0)\approx N\int_{T_0/l}^{T_0 l}P(T)dT, \tag{17}$$

where N is the total number of signals, while l is the bin size. Hence, we have obtained the critical exponent $\alpha=2.22$ [see (2)], and the correction factor parameters

$$T_c=(2.4\pm0.2)10^{-3}\ \text{sec},\quad \sigma_t=0.28\pm0.08, \tag{18}$$

where the quoted errors were estimated via 100 Monte Carlo simulations with the confidence level being equal to 0.68 [27]. In Fig. 3 we present the curve of the form (15)–(16), with T_c and σ_t given by (18) and with $\alpha=2.22$ and $B_{0t}=0.47\pm0.07$, and one can see that this curve fits the experimental data in a very satisfactory way. However, we would like to point out that the values (18) were extracted from the distribution tail, that is, for signals of long durations whose statistics is relatively meager, and, for this reason, one could expect a deviation from (18) in a experiment with a larger statistics. Similarly, it should be emphasized that the form (16) cannot stay valid in the entire region pertaining to signals of short durations (in our case, for $T<10^{-5}$ sec), so that an experiment performed in such a region would require a different correction factor.

The foregoing discussion of the duration distribution power law, (15) and (16), together with the specific assumption (8) about the elementary BN signal shape, implies a definite form for the area distribution $P(A)$. To find it, we start with the following equality

$$P(A|\gamma)dA=P(T|\gamma)dT, \tag{19}$$

which relates the conditional probabilities $P(A|\gamma)$ and $P(T|\gamma)=P(T)$ to observe a BN signal of area A and duration T (with a proviso that the signal exponent is γ), whereby one can derive the expression

$$P(A|\gamma)=\frac{1}{\gamma}B_t\left[\left(\frac{A}{C\Gamma(\gamma)}\right)^{1/\gamma}\right]\times[C\Gamma(\gamma)]^{(\alpha-1)/\gamma}A^{-[1+(\alpha-1)/\gamma]}. \tag{20}$$

Next, taking into account that $P(A)=\int P(A|\gamma)P(\gamma)d\gamma$, and since the distribution $P(\gamma)$ is narrow (see Fig. 11), one may conjecture that $P(A)$ is approximately given by the right hand side of (20) with γ being replaced by γ_1. Performing this replacement, one can recognize that (20) is, in fact, of the form (15), with

$$\tau=1+\frac{\alpha-1}{\gamma_1}, \tag{21}$$

and

$$B_a(A)=B_{0a}\exp[-(A/A_c)^{1/\sigma_a}], \tag{22}$$

where $B_{0a}=(B_{0t}/\gamma_1)[C\Gamma(\gamma_1)]^{(\alpha-1)/\gamma_1}$ and

$$A_c=C\Gamma(\gamma_1)T_c^{\gamma_1},\quad \sigma_a=\gamma_1\sigma_t. \tag{23}$$

Inserting the best fit parameters for the duration distribution (α, T_c, σ_t, and B_{0t}) in (21) and (23) one finds $\tau=1.81$, $B_{0a}=0.0144$, $A_c=7.7\times10^{-7}$ Vsec, and $\sigma_a=0.42$, whereas the best fit of the experimental data gives, respectively, $\tau=1.77\pm0.09$ [see (2)] and

$$B_{0a}=0.0141\pm0.003,\quad A_c=(6.1\pm2)\times10^{-7}\ \text{V sec},$$
$$\sigma_a=0.43\pm0.1, \tag{24}$$

which has been obtained following the same numerical procedure [27] applied in the case of the duration distribution.

In a similar way, one can obtain the scaling relation

$$\epsilon=1+\frac{\alpha-1}{2\gamma_1-1}, \tag{25}$$

for the critical exponent ϵ of the energy distribution of the BN signal, as well as the scaling relation

$$\epsilon=1+\frac{(\tau-1)(\alpha-1)}{2\alpha-\tau-1}, \tag{26}$$

that follows by eliminating γ_1 from (21) and (25). Inserting the experimental findings for α and γ_1 in (25), we obtain $\epsilon=1.61$, which is in a good agreement with the value $\epsilon=1.56$ found experimentally [see (2)]. Applying the same approach that led us to the formula (22), we obtain for the energy distribution the form of the correction factor

$$B_e(E)=B_{0e}\exp[-(E/E_c)^{1/\sigma_e}], \tag{27}$$

where

$$B_{0e}=[B_{0t}2^{1-\alpha}/(2\gamma_1-1)][C^2\Gamma(2\gamma_1-1)]^{(\alpha-1)/(2\gamma_1-1)}$$

and

$$E_c=C^2\Gamma(2\gamma_1-1)(T_c/2)^{2\gamma_1-1},\quad \sigma_e=(2\gamma_1-1)\sigma_t. \tag{28}$$

Inserting the best fit parameters for the duration distribution in (28) one finds $B_{0e}=0.004, E_c=4.0\times10^{-10}$ J, and $\sigma_e=0.56$, whereas the best fit of the experimental data gives, respectively,

$$B_{0e}=(4.3\pm0.6)\times10^{-3},\quad E_c=(4\pm2)\times10^{-10}\ \text{J},$$
$$\sigma_e=0.6\pm0.2, \tag{29}$$

which has been obtained following again the same numerical procedure [27] applied in the case of the duration distribution.

In the final part of this section, we would like to expound on our theoretical predictions about the power spectrum of the BN signal. Thus, we start with the autocorrelation function $\Psi_F(t_0)$ of the total signal $F(t)$

$$\Psi_F(t_0)=\langle F(t)F(t+t_0)\rangle=\nu\int d\gamma\int dTP(\gamma,T)\Psi_{\gamma,T}(t_0), \tag{30}$$

where

$$\Psi_{\gamma,T}(t_0)=\int_{-\infty}^{+\infty}f_{\gamma,T}(t')f_{\gamma,T}(t'+t_0)dt', \tag{31}$$

which is the autocorrelation function of the elementary signal $f_{\gamma,T}$. Therefore, the power spectrum $S(\omega)$ of the total signal $F(t)$, as a function of the angular frequency $\omega=2\pi f$, is

$$S(\omega)=\int_{-\infty}^{+\infty}\Psi_F(t_0)e^{-i\omega t_0}dt_0=\nu\langle S_{\gamma,T}(\omega)\rangle$$

$$=\nu\int d\gamma\int dTP(\gamma,T)|\hat{f}_{\gamma,T}(\omega)|^2. \tag{32}$$

Here, $S_{\gamma,T}(\omega)$ is the power spectrum of the elementary signal $f_{\gamma,T}(t')$,

$$S_{\gamma,T}(\omega)=|\hat{f}_{\gamma,T}(\omega)|^2, \tag{33}$$

and $\hat{f}_{\gamma,T}(\omega)$ is the Fourier transform of the elementary signal

$$\hat{f}_{\gamma,T}(\omega)=\int_{-\infty}^{+\infty}f_{\gamma,T}(t')e^{-i\omega t'}dt', \tag{34}$$

which for the exponentially decaying elementary signal factor $g(x)=\exp(-x)$ has the specific form [28]

$$\hat{f}_{\gamma,T}(\omega)=\frac{CT^{\gamma}\Gamma(\gamma)}{[1+(\omega T)^2]^{\gamma/2}}\exp[-i\gamma\arctan(\omega T)]. \tag{35}$$

Hence, using our assumption (8), related to the shape of elementary signals, we obtain

$$\hat{f}_{\gamma,T}(\omega)=\frac{\hat{f}_{\gamma,\omega/\omega_0 T}(\omega_0)}{\left(\frac{\omega}{\omega_0}\right)^{\gamma}},\quad \hat{f}_{\gamma,T}(\omega)=\left(\frac{T}{T_0}\right)^{\gamma}\hat{f}_{\gamma,T_0}\left(\frac{T}{T_0}\omega\right), \tag{36}$$

where we have introduced new time and frequency units T_0 and ω_0, respectively. Using the latter forms and (15) in (32) one can obtain

$$S(\omega)=\nu\int d\gamma P(\gamma)\int dT\frac{B_t\left(\frac{T}{(\omega/\omega_0)}\right)T^{-\alpha}\left|\hat{f}_{\gamma,T_0}\left(\frac{T}{T_0}\omega_0\right)\right|^2}{\left(\frac{\omega}{\omega_0}\right)^{2\gamma-\alpha+1}}\left(\frac{T}{T_0}\right)^{2\gamma}$$

$$=\nu\int d\gamma P(\gamma)\int d\left(\frac{T}{T_0}\right)T_0^{1-\alpha}\left(\frac{T}{T_0}\right)^{2\gamma-\alpha}\frac{B_t\left(\frac{(T/T_0)}{(\omega/\omega_0)}T_0\right)}{\left(\frac{\omega}{\omega_0}\right)^{2\gamma-\alpha+1}}\left|\hat{f}_{\gamma,T_0}\left(\frac{T}{T_0}\omega_0\right)\right|^2. \tag{37}$$

If we now define dimensionless quantities $\tilde{T}=T/T_0$ and $\tilde{\omega}=\omega/\omega_0$, we finally obtain our general expression for the power spectrum

$$S(\omega)=\nu T_0^{1-\alpha}\int d\gamma\frac{P(\gamma)}{\tilde{\omega}^{2\gamma-\alpha+1}}\int d\tilde{T}B_t$$

$$\times\left(\frac{\tilde{T}}{\tilde{\omega}}T_0\right)\tilde{T}^{2\gamma-\alpha}|\hat{f}_{\gamma,T_0}(\tilde{T}\omega_0)|^2. \tag{38}$$

One might conclude from (38) that the power spectrum exponent β satisfies the scaling relation

$$\beta=2\gamma_1-\alpha+1, \tag{39}$$

providing one assumes that $P(\gamma)$ can be approximated by the delta function $\delta(\gamma-\gamma_1)$ and that the integral over $\tilde{T}$ in (38) is, for high frequencies ω, approximately a constant. However, inserting data from (2) and (4) in (39) one finds that $\beta=1.80$, which deviates from the experimentally obtained value $\beta=1.6-1.7$. Therefore, in order to check the validity of the expression (38), we have evaluated $S(\omega)$ (with the time unit T_0 and the frequency unit ω_0 chosen so as to achieve stability in the corresponding numerical calculations) using (38) and approximating $P(\gamma)$ with the best fit to the Gaussian form. Results of this calculation are presented in Fig. 9 as a continuous line, whereby we have found the corresponding power-law exponent $\beta=1.67\pm0.01$. The latter value is in accord with experimental finding for β and deviates from the value $\beta=1.80$ which followed from the scaling relation (39). The deviation can be now attributed to the assumptions that have brought about (39). Hence, it appears that the integral over $\tilde{T}$ in (38) is weakly dependent on ω and γ. Besides, the second source of difference between the two values for β (1.67 vs 1.80) springs from the finite width of the $P(\gamma)$ distribution. Indeed, if we take $P(\gamma)$ to be

of a Gaussian type (instead of being a delta function), and perform the requisite lengthy calculation, we get a negative correction term on the right hand side of (39), so that instead of γ_1 there appears $\gamma_1-\sigma_\gamma^2\ln\omega$. In other words, γ_1 gets the logarithmic correction term, and if we take $\sigma_\gamma=0.05$ and, for instance, $\omega=10^5$, we get $\beta=1.74$, which is closer to the experimental finding $\beta=1.6-1.7$.

IV. DISCUSSION

In this work we have performed extensive measurements, with reliably large statistics, of the Barkhausen noise (BN) in the case of a commercial VITROVAC 6025-X metal glass sample. We have demonstrated that the BN phenomenon can be described by well defined critical exponents (see, for instance, Figs. 3–5) which satisfy a set of scaling relations. The observed power laws for the quantities T,A,E, and for their joint distributions, may be interpreted as a manifestation of the vicinity to some critical point (see, for instance, [23]). Although our findings may not be sufficient to either validate existence of the critical point, or to locate it in terms of some relevant parameters, nevertheless the established power-law behaviors, the set of scaling relations (being satisfied with our experimental findings), and the data collapsing of the type presented in Fig. 11, make us wonder whether, in the BN case, there exists also a generalized homogeneous function (GHF) with a concomitant data collapsing (in an analogy with the standard critical phenomena [29]). Here we argue, and provide evidences, that the probability distribution of BNES's is a GHF. With this goal in mind, we first introduce the scaling S_b (for $b>0$), within the set $\mathcal{B}$ of all possible BNES's, such that when it is applied to the i BNES of the shape $f_i(t')$ it gives the $S_b i$ BNES of the shape

$$f_{S_b i}(t')=b^x f_i(t'b^y), \tag{40}$$

where b is the scaling parameter, while x and y are the scaling exponents. Next, we put forward the following scaling hypothesis — if $p(i,\lambda)$ denotes the probability density to observe the i BNES when the system is at the ''distance'' λ from the critical point, then for some specific exponents (x,y) [see Eq. (40)] there exist additional exponents z and w_0 such that

$$dp(S_b i,b^z\lambda)=b^{w_0}dp(i,\lambda), \tag{41}$$

which is, in fact, the GHF statement.

To acquire possibility to verify experimentally the above GHF statement, we introduce the probability density $P(T,A,E,\lambda)$ of obtaining BNES's with given T, A, E, and λ via

$$dP(T,A,E,\lambda)=P(T,A,E,\lambda)dTdAdE=\int_{\mathcal{G}}dp(i,\lambda), \tag{42}$$

where $\mathcal{G}$ is the set of all BNES's having T, A, and E within the limits $T<T(i)<T+dT$, $A<A(i)<A+dA$, and $E<E(i)<E+dE$. Accordingly, one may prove that the probability density $P(T,A,E,\lambda)$ is the generalized homogeneous function

$$P(b^{-y}T,b^{x-y}A,b^{2x-y}E,b^z\lambda)=b^wP(T,A,E,\lambda), \tag{43}$$

where

$$w=w_0-3(x-y), \tag{44}$$

which, with $\tilde{z}=z/y$ and $\tilde{w}=w/y$, and with the another scaling parameter $c=b^{-y}$, can be rewritten in a more convenient form,

$$P(cT,c^{a_A}A,c^{a_E}E,c^{a_\lambda}\lambda)=c^{a_P}P(T,A,E,\lambda), \tag{45}$$

where

$$a_A=1-\tilde{x},\quad a_E=1-2\tilde{x},\quad a_\lambda=-\tilde{z},\quad a_P=-\tilde{w}. \tag{46}$$

To prove (43), we start with the auxiliary relations between the duration T, area A, energy E, and Fourier transform $\hat{f}(\omega)$ of the original i BNES and the scaled $S_b i$ BNES,

$$T(S_b i)=b^{-y}T(i), \tag{47a}$$

$$A(S_b i)=b^{x-y}A(i), \tag{47b}$$

$$E(S_b i)=b^{2x-y}E(i), \tag{47c}$$

$$\hat{f}_{S_b i}(\omega)=b^{x-y}\hat{f}_i(\omega b^{-y}), \tag{47d}$$

which can be verified in few steps. Indeed, to obtain (47a), one has to notice that the duration T of BNES is defined by $T=t_l-t_f$, where t_f and t_l are the first and the last moments, respectively, of the time interval when BNES is above the discrimination level b_d. Besides, one has to keep in mind that T displays only minor changes if the discrimination level b_d is changed. Thus, one can make the choice $b_d=b_l+\delta_d b^x$ (see Sec. II B), in the case of the scaled $S_b i$ BNES, and thereby one obtains (47a). In order to obtain (47b)–(47d), one has to perform the change of the variable $t\to t'=b^y t$ in the integrals which appear in definitions of A, E, and $\hat{f}(\omega)$, given in Sec. III. Next, we return to the proof of (43), and to this end we write

$$P(b^{-y}T,b^{x-y}A,b^{2x-y}E,b^z\lambda)=\frac{dP(b^{-y}T,b^{x-y}A,b^{2x-y}E,b^z\lambda)}{d(b^{-y}T)d(b^{x-y}A)d(b^{2x-y}E)}=\frac{\int_{\mathcal{G}'}dp(i,b^z\lambda)}{b^{3(x-y)}dTdAdE}, \tag{48}$$

where S_b image of $\mathcal{G}$ is the set $\mathcal{G}'$ of all BNES's having T, A, and E within the limits $b^{-y}T<T(i)<b^{-y}(T+dT)$, $b^{x-y}A<A(i)<b^{x-y}(A+dA)$, and $b^{2x-y}E<E(i)<b^{2x-y}(E+dE)$. Then, using (41) and the relation

$$\int_{\mathcal{G}'}dp(i,b^z\lambda)=\int_{\mathcal{G}}\frac{dp(S_b i,b^z\lambda)}{dp(i,\lambda)}dp(i,\lambda)=b^{w_0}\int_{\mathcal{G}}dp(i,\lambda), \tag{49}$$

one obtains (43).

In what follows we are going to demonstrate that the power laws (1) for the $P(T)$, $P(A)$, and $P(E)$ distributions,

and all scaling relations of Sec. III, can be obtained from (43) if one chooses the scaling exponents a_A, a_E, a_λ, and a_P in the following way:

$$a_P=-\frac{\epsilon\alpha\tau+2-\epsilon-\alpha-\tau}{(1-\tau)(1-\epsilon)},\quad a_A=\frac{1-\alpha}{1-\tau},\quad a_E=\frac{1-\alpha}{1-\epsilon},$$

$$a_\lambda=1/\sigma_T, \tag{50}$$

where α, τ, and ϵ are the scaling exponents of (1) and σ_T is the exponent of (16). Indeed, for the duration distribution $P(T)$ we have

$$P(T)=\int dA\int dE P(T,A,E,\lambda)$$
$$=T^{a_P+a_A+a_E}\int d\left(\frac{A}{T^{a_A}}\right)\int d\left(\frac{E}{T^{a_E}}\right)P\left(1,\frac{A}{T^{a_A}},\frac{E}{T^{a_E}},\frac{\lambda}{T^{a_\lambda}}\right), \tag{51}$$

whereby one can see that $P(T)$ exhibits a power-law behavior, with the correction term (given by the integral of the last relation) and with the scaling exponent α given by

$$\alpha=-(a_P+a_A+a_E). \tag{52}$$

In a similar way, one can show that the distributions $P(A)$ and $P(E)$ obey power-law behavior as well, with the exponents τ and ϵ given by

$$\tau=-\frac{a_P+a_E+1}{a_A},\quad \epsilon=-\frac{a_P+a_A+1}{a_E}. \tag{53}$$

Finally, starting with Eqs. (52) and (53), one can obtain the first three relations of (50). As regards the correction term of the power law (16), one may conjecture that the fourth relation of (50) stays valid and that the cutoff parameter T_c of (16) might serve as the parameter λ which measures distance from the critical point (at which the system should exhibit the pure power laws, with the cutoffs removed). As to the stretched-exponential form (16) for the correction term, we can say that this form (being specific) does not follow from the general scaling hypothesis (41).

The power laws of the form (3) also follow from the scaling hypothesis (41) with the identification

$$\gamma_1=a_A,\quad \gamma_2=a_E,\quad \gamma_3=a_E/a_A, \tag{54}$$

between the set of experimental exponents γ_1, γ_2, and γ_3 and the set of theoretical exponents a_A and a_E, which can be verified by recalling that the average area $\langle A\rangle_T$ of the BNES's, of the duration T, satisfies

$$\langle A\rangle_T=\frac{\int dA\int dE P(T,A,E,\lambda)A}{\int dA\int dE P(T,A,E,\lambda)}$$
$$=T^{a_A}\frac{\int dv_2 v_2\int dv_3 P(1,v_2,v_3,\lambda/T^{a_\lambda})}{\int dv_2\int dv_3 P(1,v_2,v_3,\lambda/T^{a_\lambda})}, \tag{55}$$

whereby the first equality of (54) follows. The remaining two equalities of (54) follow in analogous way. Then, combining the first two relations of (46), the second and the third relation of (50), and (54), we retrieve the scaling relations (14), (21), and (25). In a similar way one may also derive relations (23) and (28), with the remark that A_c and E_c might also play the role of the parameter λ.

To make the present derivation of the scaling relations complete, we are going to rederive the scaling relation (39), which relates the exponent γ_1 and the duration exponent α with the exponent β of the power spectrum. To this end, we start with

$$S(\omega)=\nu\int dp(i,\lambda)|\hat{f}_i(\omega)|^2$$
$$=\nu\int dT\int dA\int dE P(T,A,E,\lambda)\frac{\int_{\mathcal{G}}dp(i,\lambda)|\hat{f}_i(\omega)|^2}{\int_{\mathcal{G}}dp(i,\lambda)}, \tag{56}$$

and use (43), together with

$$\int_{\mathcal{G}}dp(i,\lambda)=\int_{S_{b^{-1}}(S_b\mathcal{G})}dp(i,(b^{-1})^z\lambda')$$
$$=\int_{\mathcal{G}'}\frac{dp(S_{b^{-1}}i',(b^{-1})^z\lambda')}{dp(i',\lambda')}dp(i',\lambda')$$
$$=b^{-w_0}\int_{\mathcal{G}'}dp(S_b i,b^z\lambda), \tag{57}$$

where $\lambda'=b^z\lambda$ and $i'=S_b i$, and

$$\int_{\mathcal{G}}dp(i,\lambda)|\hat{f}_i(\omega)|^2$$
$$=b^{2(y-x)-w_0}\int_{\mathcal{G}'}dp(S_b i,b^z\lambda)|\hat{f}_{S_{b^i}}(b^y\omega)|^2, \tag{58}$$

to obtain

$$S(\omega)=\nu b^{2(y-x)-w}\int dT\int dA$$
$$\times\int dE P(b^{-y}T,b^{x-y}A,b^{2x-y}E,b^z\lambda)$$
$$\times\frac{\int_{\mathcal{G}'}dp(S_b i,b^z\lambda)|\hat{f}_{S_{b^i}}(b^y\omega)|^2}{\int_{\mathcal{G}'}dp(S_b i,b^z\lambda)}, \tag{59}$$

which for $b=\omega^{-1/y}$, and with the rescaled variables $v_1=\omega T$, $v_2=\omega^{\gamma_1}A$, and $v_3=\omega^{\gamma_2}$, becomes

$$S(\omega)=\nu\omega^{-(2\gamma_1-\alpha+1)}\int dv_1\int dv_2$$
$$\times\int dv_3 P(v_1,v_2,v_3,\omega^{\tilde{z}}\lambda')$$
$$\times\frac{\int_{\mathcal{G}'}(i',\omega^{\tilde{z}}\lambda')|\hat{f}_{i'}(1)|^2}{\int_{\mathcal{G}'}(i',\omega^{\tilde{z}}\lambda')}. \tag{60}$$

Hence, we can see that (39) can be obtained also within the GHF approach.

Having verified that the scaling relations obtained in the Sec. III follow also from the GHF hypothesis (41), we are going to show that this hypothesis, as could have been expected, implies data collapsing in the case of the probability distribution functions. Indeed, performing suitable integration of the distribution $P(T,A,E,\lambda)$ and with a change of variables one can find

$$P(A,T)T^{\alpha+\gamma_1}=\varphi_1(A/T^{\gamma_1})=\int dv_3 P\left(1,\frac{A}{T^{\gamma_1}},v_3,\frac{\lambda}{T^{a_\lambda}}\right), \tag{61}$$

$$P(E,T)T^{\alpha+\gamma_2}=\varphi_2(E/T^{\gamma_2})=\int dv_2 P\left(1,v_2,\frac{E}{T^{\gamma_2}},\frac{\lambda}{T^{a_\lambda}}\right), \tag{62}$$

$$P(E,A)A^{\tau+\gamma_3}=\varphi_3(E/A^{\gamma_3})=\int dv_1 P\left(v_1,1,\frac{E}{A^{\gamma_3}},\frac{\lambda}{A^{a_\lambda/\gamma_1}}\right), \tag{63}$$

which are correct for a fixed λ, and may be correct also in the case of a weak dependence on λ.

The first approach one might have in mind in order to check whether our experimental data collapse in accordance with the above relations is to study the quantity $N_l(A_0,T_0)T_0^{\tau+\gamma_1}$, where $N_l(A_0,T_0)=N\int dT\int dA P(A,T)$ is the number of elementary signals which belong to a linear bin centered at the values A_0 and T_0. Such a procedure is, however, inconvenient since the relevant distributions are of a power-law type, so that all data practically lie in the first linear bin. Therefore, in order to group experimental data in a suitable form, one has to separate data in the logarithmically spaced bins, that is, to integrate $NP(A,T)T^{\alpha+\gamma_1}$ within the limits $A_0/\delta A<A<A_0\delta A$ and $T_0/\delta T<T<T_0\delta T$, where δA and δT determine the size of a logarithmic bin. In such a way one obtains the following data-collapsing relations:

$$N(A,T)T^{\alpha-1}=\phi_1(A/T^{\gamma_1}), \tag{64}$$

$$N(E,T)T^{\alpha-1}=\phi_2(E/T^{\gamma_2}), \tag{65}$$

$$N(E,A)A^{\tau-1}=\phi_3(E/A^{\gamma_3}), \tag{66}$$

where, for instance,

$$\phi_1(A_0/T_0^{\gamma_1})=\int_{A_0/T_0\delta A}^{A_0\delta A/T_0} dv\,\varphi_1(v). \tag{67}$$

In Figs. 12–14 we present our experimental data scaled according to the relations (64)–(66), respectively. In each case the data have been taken from four different ''channels,'' that is, from four different families of logarithmic bins defined by four corresponding values of T_0 and A_0, which belong to the pertinent power-law regions of Figs. 3 and 4. It follows that the degree of data collapsing depends on the choice of values for the critical exponents. Thus, one could argue that the choice of the critical exponents values which produces the best data collapsing is the most proper choice for the problem under study. Furthermore, one could claim that such a choice is, in fact, the best way to evaluate critical exponents. However, such a procedure of obtaining critical exponents involves a very intricate numerical calculations

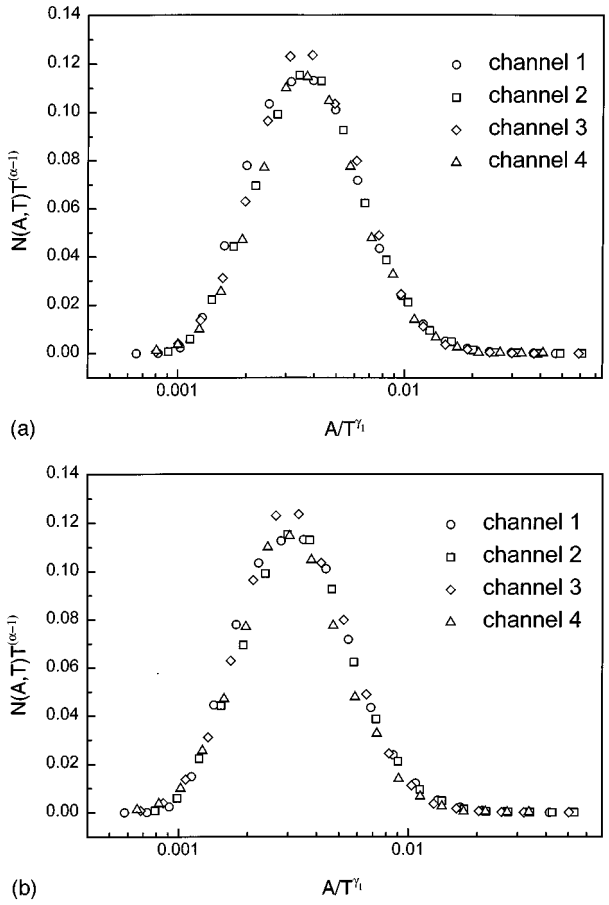

FIG. 12. (a) Data collapsing of the quantity $N(A,T)$, which is related to the probability density function through the relation (64), with the exponents $\alpha=2.22$ and $\gamma_1=1.51$ which were reported in Sec. II. (b) Data collapsing of the quantity $N(A,T)$, obtained with the exponents $\alpha=2.22$ and $\gamma_1=1.55$ which were chosen so as to produce visually the best data collapsing, that is, collapsing with the least possible scattering of the data points from a single curve. In both cases (a) and (b), the $N(A,T)$ data were taken from four T channels which belong to the scaling region of duration distribution (cf. Fig. 3). More specifically, the channels 1–4 correspond to the following values of T_0 (in secs) 9.72×10^{-5}, 1.59×10^{-4}, 2.61×10^{-4}, and 7.03×10^{-4}, respectively, while the ''halfwidth'' of a channel is $\delta T=1.28$, which reflects a choice of 14 channels on the entire duration axis of Fig. 3.

which definitely increases uncertainty of final results. For instance, in the present case, according to the foregoing procedure [whose final results are depicted in Figs. 12(b), 13(b), and 14(b)], we have found the following set: $\alpha=2.22$, $\gamma_1=1.55$, $\gamma_2=2.15$, $\gamma_3=1.46$, and $\tau=1.68$ (in which only the critical exponent α coincides with the straightforward measurement, whereas the rest are somewhat changed). This set of exponents, unfortunately, does not satisfy the scaling relations to the same degree which was observed in the case of critical exponents derived directly from the joint distributions. The discrepancy may be ascribed to the accumulated numerical error during the course of determination of data that were finally scaled, as well as to the possibility that the entire experiment was not performed close enough to the assumed critical point (which could have brought about inaccurate critical exponents). In short, the above set of values

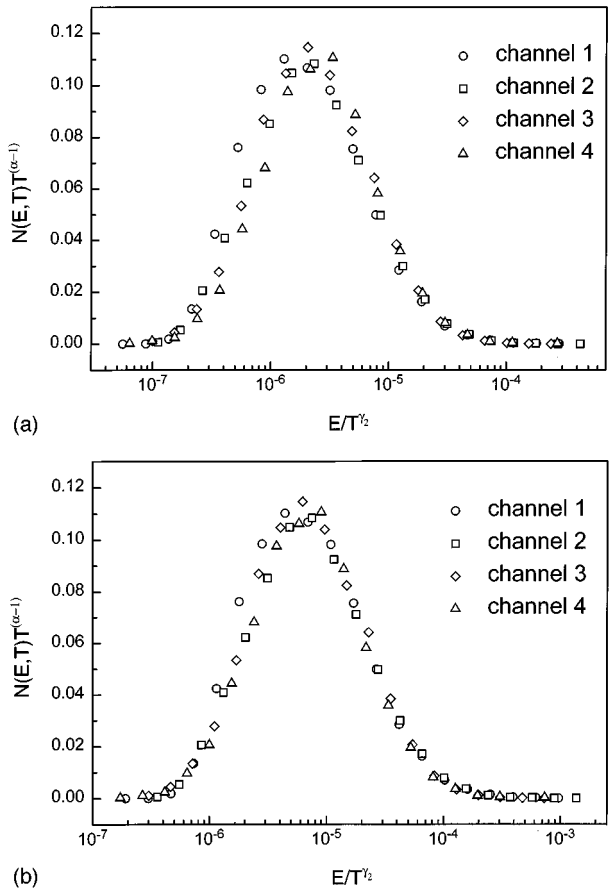

FIG. 13. (a) Data collapsing of the quantity $N(E,T)$, which is related to the probability density function through the relation (65), with the exponents $\alpha=2.22$ and $\gamma_2=2.03$ which were reported in Sec. II. (b) Data collapsing of the quantity $N(E,T)$, obtained with the exponents $\alpha=2.22$ and $\gamma_2=2.15$ which were chosen so as to produce visually the best data collapsing, that is, collapsing with the least possible scattering of the data points from a single curve. Here, the comment about the channels, made in Fig. 12, stays valid too.

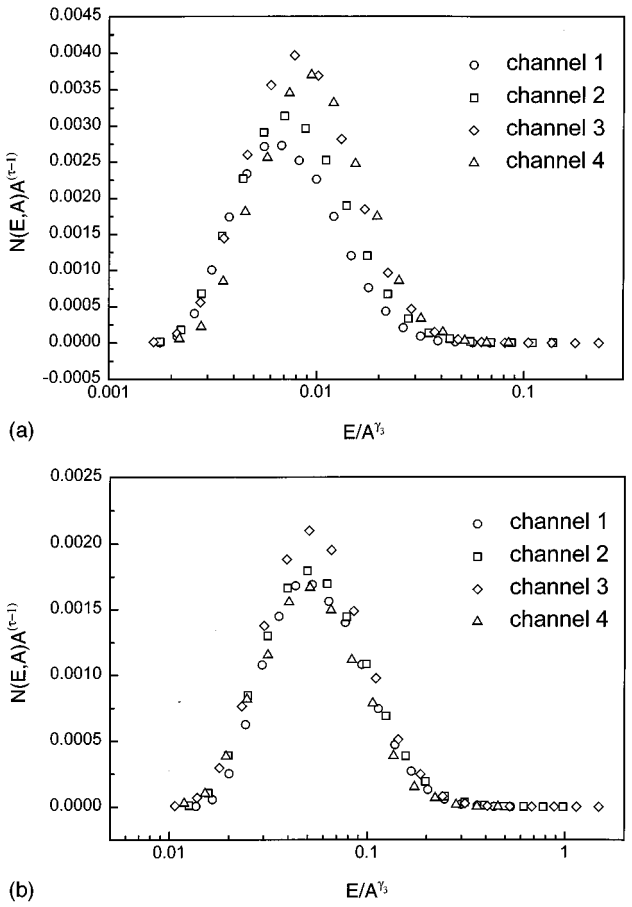

FIG. 14. (a) Data collapsing of the quantity $N(E,A)$, which is related to the probability density function through the relation (66), with the exponents $\tau=1.77$ and $\gamma_3=1.36$ which were reported in Sec. II. (b) Data collapsing of the quantity $N(E,A)$, obtained with the exponents $\tau=1.68$ and $\gamma_3=1.46$ which were chosen so as to produce visually the best data collapsing, that is, collapsing with the least possible scattering of the data points from a single curve. In both cases (a) and (b), the $N(E,A)$ data were taken from four A channels which belong to the scaling region of area distribution (cf. Fig. 4). More specifically, the channels 1–4 correspond to the following values of A_0 (in V sec) 1.24×10^{-9}, 3.01×10^{-9}, 7.30×10^{-9}, and 4.29×10^{-8}, respectively, while the ''halfwidth'' of a channel is $\delta A=1.56$, which reflects a choice of 14 channels on the entire area axis of Fig. 4.

of critical exponents should be accepted cautiously, together with the message that they have played an important role in demonstrating that BN exhibits the basic element of the traditional critical phenomena, that is, the data collapsing property.

The preceding discussion about the GHF concept imposes the question as to which of the two approaches (the one presented in Sec. III and the GHF approach) should be undertaken in the further BN study. To our minds, both approaches have their own benefits and both of them should be performed. The GHF concept should be studied further in order to clarify the type of the critical phenomena relevant to BN. On the other hand, the well established generic shape of BNES's (see Fig. 10) should bear definite amount of information about the mesoscopic dynamic of magnetic domain behavior (reflecting material characteristics), and, for this reason, it deserves to be pursued in the future.

After the long discussion about the theoretical presentation of obtained results, we now elaborate on few subtle experimental problems and the way we have treated them in order to achieve the correct picture of BN. First, in order to minimize distortions of BN, we have used a sufficiently long pickup coil which entirely enclosed the ferromagnetic specimen studied, and, in addition, we have carefully analyzed characteristics of the amplifier used, which enabled us to eliminate the concomitant distortions that it brought about. Without these two precautions one cannot obtain clear power-law characteristics of BN. Second, we have been concerned about the possibility of extending the observed BN power laws (see Figs. 3–5) in the regions of small values of the relevant arguments. With respect to this problem, we note that, despite the presence of a rather good magnetic shielding and the signal amplification in the very vicinity of the pickup coil (see Fig. 1), our experimental conditions were marked by the extrinsic high-frequency noise (which appeared for the frequencies higher than 50 kHz). Because of this, we may conclude that to assess the initial behavior of

the BN power laws, one would have to reduce the extrinsic noise, and, to accomplish this, one would have to use a more effective magnetic shielding and a faster A/D converter (with a better resolution).

In the introductory part of this paper, it has been pointed out that BN has many different facets under various experimental conditions, even for the single ferromagnetic sample. Thus, one generally finds that, if the driving frequency is high enough, the BN elementary signals (that originate form the spatially separated regions of the ferromagnetic sample under study) are glued, whereas if the driving frequency is low enough BN appears as a train of pulses mutually well separated (by time intervals in which only external noise is observed). Therefore, in the latter case, it is plausible to identify experimentally discernible single BN signals with BN elementary signals. In order to observe experimentally well separated BN elementary signals, we have chosen the driving frequency of 0.03 Hz. This frequency, on the one hand, lies in the frequency region where statistical characterization of BN remains stable under frequency variation (i.e., it is low enough) and, on the other hand, it is high enough to permit efficient collection of BN data.

With respect to the question of the numerical values for the power laws exponents obtained by other authors, we would like first to mention that the BN exponents reported so far do not exhibit universality. Next, our experimental conditions were close to the experimental conditions arranged by Cote and Meisel [16] for the Metglas sample, but our results are more close to the exponents they have found for Alumel, in which case the scaling relation (26) is fulfilled as well. Likewise, it is interesting that the relation (26) is exactly satisfied by the exponents quoted in [24] and that our power-law exponent values are not very different from those obtained in [24]. The major difference, however, appears in the case of power-spectrum exponent β. Meisel and Cote [16] insisted on the value $\beta=2$, emphasizing the Brownian character of the observed BN, whereas Perković *et al.* [24] have found the value $\beta=2.46$, for the spectrum in a small bin, and $\beta=1.70$, for the spectrum of the entire hysteresis loop. Our finding $\beta=1.6-1.7$, for which we claim that it is not decreased by the aliasing effect, is more close to the value reported in [20,21] and to some earlier findings [3]. On the other hand, the scaling relation (39), for which we have argued that should contain a correction term, is satisfied for the numerical results found for the zero-temperature random-field Ising model [24], and it is approximately satisfied for the experimental results obtained by Meisel and Cote [16].

In conclusion, the foregoing specific comparisons show that the scaling relations established in this paper are much better satisfied in the case of results obtained within the numerical simulations [24] of the RFI model (which promotes the ''plain old criticality'' for the explanation of BN), than in the case of the experimental work [16], which first advocated the SOC model and afterwards [17] allowed of different interpretations of BN. On the other hand, the power-law exponents found in this work are in a better agreement with those reported in the experimental work [16] than with those predicted via the numerical simulations [24]. It is hard, on these grounds, to recognize which of the two models (the RFI or the SOC model) gives a more correct elucidation of BN. However, it was not the aim of the present paper to provide means for choosing the most adequate model for BN, but rather to point out the role of BNES's, power laws, scaling relations, and the data collapsing, in an attempt to understand the criticality of BN.

ACKNOWLEDGMENTS

The first two authors would like to acknowledge cordial help provided by Biljana Radojević, Dragan Kotri, and Ljuba Zavlaković, in the experimental part of this work. Besides, one of the authors (S.M.) would like to express his gratefulness to Brigita Kutnjak-Urbanc and Stefano Zapperi for many helpful discussions on topics related to the problem studied in this work. The Center for Polymer Studies is supported by grants from the NSF.

[1] H. Barkhausen, Phys. Z. **20**, 401 (1919).
[2] H. Bittel, IEEE Trans. Magn. **5**, 359 (1969).
[3] H. Bittel, Physica B **83**, 6 (1976).
[4] J. C. McGlure, Jr. and K. Schröder, CRC Crit. Rev. Solid State Sci. **6**, 45 (1976).
[5] H. N. Bertram and J. G. Zhu, in *Solid State Physics: Advances in Research and Applications*, edited by H. Ehrenreich and D. Turnbull (Academic Press, San Diego, 1992), Vol. 46.
[6] L. B. Sipahi, J. Appl. Phys. **75**, 6978 (1994).
[7] B. Alessandro, C. Beatrice, G. Bertotti, and A. Montorsi, J. Appl. Phys. **68**, 2901 (1990); **68**, 2908 (1990).
[8] C. Beatrice and G. Bertotti, J. Magn. Magn. Mater. **104-107**, 324 (1993).
[9] R. D. McMichael, L. J. Swartzendruber, and L. H. Bennett, J. Appl. Phys. **73**, 5848 (1993).
[10] G. Bertotti, G. Durin, and A. Magni, J. Appl. Phys. **75**, 5490 (1994).
[11] G. Bertotti, in *Noise in Physical Systems and 1/f Fluctuations*, edited by P. H. Handel and A. L. Chung (American Institute of Physics, New York, 1993).
[12] G. Bertotti, in *Models of Hysteresis*, edited by A. Visintin (Longman Scientific & Technical, Harlow, 1993).
[13] A. Kirilyuk, J. Ferré, and D. Renard, Europhys. Lett. **24**, 403 (1993).
[14] P. Bak, C. Tang, and K. Wiesenfeld, Phys. Rev. Lett. **59**, 381 (1987); Phys. Rev. A **38**, 364 (1988).
[15] P. Bak and M. Creutz, in *Fractals in Science*, edited by A. Bunde and S. Havlin (Springer-Verlag, New York, 1994).
[16] P. J. Cote and L. V. Meisel, Phys. Rev. Lett. **67**, 1334 (1991); L. V. Meisel and P. J. Cote, Phys. Rev. B **46**, 10 822 (1992).
[17] P. J. Cote and L. V. Meisel, Int. J. Mod. Phys. B **7** 934 (1993).
[18] H. J. Jensen, K. Christensen, and H. C. Fogedby, Phys. Rev. B **40**, 7425 (1989); K. Christensen, C. H. Fogedby, and H. J. Jensen, J. Stat. Phys. **63**, 653 (1991).
[19] K. L. Babcock and R. M. Westervelt, Phys. Rev. Lett. **64**, 2169 (1990).

[20] O. Geoffroy and J. L. Portseil, J. Magn. Magn. Mater. **97**, 198 (1991); **97**, 205 (1991).
[21] O. Geoffroy and J. L. Portseil, J. Magn. Magn. Mater. **133**, 1 (1994).
[22] K. P. O'Brien and M. B. Weissman, Phys. Rev. A **46** R4475 (1992); Phys. Rev. E **50**, 3446 (1994).
[23] J. P. Sethna, K. Dahmen, S. Kartha, J. A. Krumhansl, B. W. Roberts, and J. D. Shore, Phys. Rev. Lett. **70**, 3347 (1993); K. Dahmen and J. P. Sethna, *ibid.* **71**, 3222 (1993); K. Dahmen, S. Kartha, J. A. Krumhansl, B. W. Roberts, J. P. Sethna, and J. D. Shore, J. Appl. Phys. **75**, 5946 (1994).
[24] O. Perković, K. Dahmen, and J. P. Sethna, Phys. Rev. Lett. **75**, 4528 (1995).
[25] K. Dahmen and J. P. Sethna, Phys. Rev. B **53**, 14 872 (1996).
[26] J. S. Urbach, R. C. Madison, and J. T. Markert, Phys. Rev. Lett. **75**, 276 (1995).
[27] W. H. Press, B. P. Flannery, S.A. Teukolsky, and W. T. Vetterling, *Numerical Recipes* (Cambridge University Press, Cambridge, 1990).
[28] A. P. Prudnikov, Yu. A. Brychkov, and O. I. Marychev, *Integrals and Series* (Nauka, Moscow, 1981) (in Russian).
[29] H. Eugene Stanley, *Introduction to Phase Transitions and Critical Phenomena* (Clarendon Press, Oxford, 1971).